Int. J. Electrochem. Sci., 14 **(2019)** 1178 – 1196, doi: 10.20964/2019.02.06

International Journal of
ELECTROCHEMICAL
SCIENCE
www.electrochemsci.org

Solanum lasiocarpum L. Extract as Green Corrosion Inhibitor for A3 Steel in 1 M HCl Solution

Xia Wang[*], *Huan Jiang*[*], *Dai-xiong Zhang, Li Hou, Wen-jie Zhou*

School of Material Science and Engineering, Southwest Petroleum University, Chengdu 610500, People's Republic of China
[*]Email: swpi_wx@126.com, jiangqingze6379@163.com

Received: 3 August 2018 / *Accepted:* 28 November 2018 / *Published:* 5 January 2019

An extract of Solanum lasiocarpum L. (SL) was characterized and tested for its potential anticorrosion effect on A3 steel in a 1 M HCl solution using weight loss analysis, potentiodynamic polarization measurements, electrochemical impedance spectroscopy, Fourier transform infrared spectroscopy and scanning electron microscopy (SEM). The electrochemical and weight loss results revealed that the SL extract was an efficient corrosion inhibitor with an inhibition efficiency of up to 93.31% at a concentration of 1 g/L, which was further confirmed by SEM observations. The adsorption process mainly comprised physisorption and chemisorption (comprehensive adsorption), and obeyed the Langmuir model. The SL extract is a mixed inhibitor that predominantly suppresses the cathodic reaction.

Keywords: Solanum lasiocarpum L., Plant-based corrosion inhibitor, Adsorption, Electrochemical

1. INTRODUCTION

As an efficient method for cleaning metal surfaces, acid pickling has been widely used for removing scale and rust from surfaces, for example, by dipping steel into an acidic solution[1]. The employment of an acid to clean rust and dirt from a metal surface is an important means of pretreating metal surfaces and descaling pipelines and boiler systems and has been widely used in the maintenance of metallic materials and machinery, metallurgy, the chemical industry and other industries[2]. Owing to the corrosive nature of acids, an over-etching phenomenon often occurs in the acid pickling process; that is, not only is the surface cleaned by the removal of corrosion and dirt, but also part of the metal substrate is washed away at the same time[3]. Therefore, the acid pickling process not only causes the dissolution of the metal and wastes the acid pickling solution but also produces a large amount of acid pickling waste, which causes serious environmental pollution. In order to suppress the dissolution of the metal, a

corrosion inhibitor is generally added to the acidic solution in a low concentration. If the corrosion inhibitor has high toxicity, it will inevitably result in secondary pollution[4]. Therefore, an environmentally friendly corrosion inhibitor is a critical requirement in acid pickling and cleaning. In addition, with regard to the requirements for resource savings and environment-friendliness, some conventional corrosion inhibitors are poisonous, harmful and polluting, and hence their use is restricted and/or prohibited[5]. However, corrosion inhibitors of plant origin have a wide range of sources and are non-polluting, non-toxic etc., and hence they will gradually be developed and widely used in the pickling industry[6,7].

Some researchers have studied the corrosion-inhibiting activity of flavonoids in lotus leaves and found that these flavonoids are strongly adsorbed on metals; that is, these flavonoids exhibit good corrosion inhibition[8]. The fruit of Solanum lasiocarpum L. (SL) is very rich in flavonoids[9,10], and hence SL may have the potential to be a corrosion inhibitor. Moreover, it has a wide range of sources and is abundant in production.

This work represents the first study of the corrosion-inhibiting effect of an SL extract on A3 steel in a 1 mol/L HCl solution. The corrosion behaviour of A3 steel in the 1 M HCl solution with and without the SL extract was studied using weight loss measurements, potentiodynamic polarization and electrochemical impedance spectroscopy. The chemical structure of the extract was characterized by Fourier transform infrared spectroscopy (FTIR), and thermodynamic and kinetic data were obtained via weight loss analysis. The surface morphology of the A3 steel was characterized by scanning electron microscopy (SEM).

2. EXPERIMENTAL

2.1. Preparation of material samples

The samples used in this experiment comprised A3 steel, and their chemical composition was 0.22 wt% C, 0.3 wt% Si, 0.14 wt% Mn, 0.045 wt% P, 0.01 wt% Ni, 0.01 wt% Cr and the remainder Fe. Their density was 7.85 g/cm^3. The A3 steel specimens were cut into pieces with dimensions of 3 cm × 1.5 cm × 0.2 cm for the weight loss measurements. The working electrode used in the electrochemical tests comprised A3 steel; that is, the sample was sealed with epoxide resin, and the working surface that was reserved had dimensions of 1 cm × 1 cm.

2.2. Preparation of SL extract

SL was collected in Luzhou, Sichuan province, China. Soaking extraction and ultrasound extraction were employed to obtain the SL extract, and distilled water was used as the extraction solvent in this experiment. The SL was decontaminated, washed, dried in a dry oven at 313 K, ground and finally stored in a sealed bag for later use.

To devise an optimal scheme for the preparation of the SL extract, the $L_9(3^4)$ orthogonal design method was used for optimization. In the extraction method that was used, the soaking temperature,

soaking time and ultrasound time are the key experimental factors that affect the efficiency of extraction. Therefore, each of these factors was set at three levels, as shown in Table 1.

Table 1. Orthogonal design table of factors and levels

Level	Factor		
	A-soaking temperature （K）	B-soaking time（h）	C-ultrasound time （min）
1	303	8	20
2	323	16	40
3	343	24	60

2.3. Fourier transform infrared spectroscopy (FTIR)

In this experiment, FTIR was used to characterize the SL extract. According to the positions of the absorption peaks, the chemical bond that corresponded to each absorption peak was preliminarily estimated, and functional groups with adsorption properties were examined to determine whether they had corrosion-inhibiting properties.

2.4. Weight loss method

The A3 steel samples were immersed in a 1 M HCl solution containing different concentrations of SL extract (0.2–1 g/L) at different temperatures (30–60 °C) for 4 h. After immersion, the specimens were removed from the solution, rinsed with distilled water, washed with acetone, dried thoroughly and weighed. The mass of the A3 steel specimens before and after immersion was determined using an analytical balance with a precision of 0.1 mg. Three parallel experiments were performed under the same experimental conditions, and then the data with no significant errors were averaged. The mass loss (w) was used to calculate the inhibition efficiency (η) as follows:

$$\eta = \frac{v_{corr}^{0} - v_{corr}^{inh}}{v_{corr}^{0}} \times 100\% \quad (1)$$

Where V_{corr}—— corrosion rate, $g \cdot m^{-2} \cdot h^{-1}$

The corrosion rate (V_{corr}) of A3 steel was calculated using the formula:

$$V_{corr} = \frac{w_0 - w_1}{St} \quad (2)$$

where w_0 —— the quality of A3 steel before corrosion, g

w_1—— quality of A3 steel after corrosion, g

S —— surface area of the sample, m^2

t —— corrosion time, h

2.5. Electrochemical measurements

In the electrochemical experiments, impedance spectra and polarization curves were recorded using a CS electrochemical workstation. The electrochemical tests used a conventional three-electrode system, and the experimental temperature was controlled by a constant-temperature water bath. In the three-electrode system, a platinum electrode was used as the auxiliary electrode, a saturated calomel electrode was used as the reference electrode and an A3 steel sample was used as the working electrode. All the electrochemical tests were performed at a temperature of 303 K. Electrochemical impedance tests were performed first, and the scanning frequency ranged from 100 kHz to 10 mHz with an amplitude of 5 mV. Then, potentiodynamic scanning was performed over the scanning range of −0.2 V–0.2 V (relative to open-circuit potential) at a scanning speed of 0.5 mV/s. From the Nyquist plot of the real versus imaginary impedance (Z_{real} vs $Z_{imaginary}$), electrochemical parameters such as the charge transfer resistance (R_{ct}) and double-layer capacitance (C_{dl}) were calculated. The corrosion potential (E_{corr}), corrosion current density (I_{corr}) and anodic (β_a) and cathodic (β_c) Tafel slopes were also calculated.

$$\eta\ (\%) = \frac{I_{corr}^{0} - I_{corr}^{inh}}{I_{corr}^{0}} \times 100\% \qquad (3)$$

where I_{corr}^{0} —— corrosion current density without added corrosion inhibitor

I_{corr}^{inh} —— corrosion current density added to corrosion inhibitor

Calculating the corrosion inhibition rate η using charge transfer resistance can be as follows:

$$\eta(\%) = \frac{R_{ct}^{inh} - R_{ct}^{0}}{R_{ct}^{inh}} \times 100\% \qquad (4)$$

where R_{ct}^{0} —— charge transfer resistance of blank solution

R_{ct}^{inh} —— charge transfer resistor after adding corrosion inhibitor

2.6. SEM analysis

A3 steel samples were immersed in a 1 M HCl solution containing SL extracts with concentrations of 0, 0.2 and 1 g/L for 4 h. After immersion, the A3 steel samples were removed, cleaned and dried with acetone and absolute alcohol. SEM was used to observe the corrosion morphology of the A3 steel surface, and the corrosion mechanism was estimated by combining the corrosion morphology with the electrochemical test results.

3. RESULTS AND DISCUSSION

3.1 Optimization of extraction conditions

In order to devise the best scheme for the preparation of the SL extract, nine different preparation schemes were designed using an $L_9(3^4)$ orthogonal design table, as shown in Table 2. The corrosion inhibition efficiencies achieved using these nine different preparation schemes are shown in Table 2, and the effects of changes in the levels of the various experimental factors on the corrosion inhibition efficiency were analyzed. K_{ij} represents the sum of all the experimental results for level i in column j, k_{ij}

represents the corresponding average value of K_{ij} and R is the range between the maximum and minimum values of K_{ij}.

$$k_{ij} = \frac{K_{ij}}{3} \quad (5)$$

$$R = \max\left(K_{ij}\right) - \min\left(K_{ij}\right) \quad (6)$$

According to the results listed in Table 2, $R_1 > R_2 > R_3$. This indicates that the soaking temperature was more important than the soaking time and the soaking time was more important than the ultrasound time. From the values of K_{ij}, the third level of factor A, the second level of factor B and the third level of factor C were selected and combined as the optimal scheme for preparing the SL extract. Therefore, the optimal scheme for the preparation of the SL extract comprised a soaking temperature of 343 K, a soaking time of 16 h and an ultrasound time of 60 min. In the following sections, the SL extract solution that was used was prepared by this optimal scheme.

Table 2. Orthogonal design table

NO.	Factor			contents
	A-soaking temperature(K)	B-soaking time(h)	C-ultrasound time(min)	η%
1	303	8	20	80.7
2	303	16	40	84.7
3	303	24	60	82.1
4	323	8	40	83.6
5	323	16	60	89.2
6	323	24	20	86.8
7	343	8	60	85.4
8	343	16	20	87.9
9	343	24	40	86.3
K_1	2.4747	2.4971	2.5538	
K_2	2.5954	2.6179	2.5462	
K_3	2.5966	2.5517	2.5667	
k_1	0.8249	0.8324	0.8513	
k_2	0.8651	0.8726	0.8487	
k_3	0.8655	0.8506	0.8556	
R_j	0.0406	0.0402	0.0069	

3.2 Fourier transform infrared spectroscopy (FTIR)

The FTIR spectrum of the SL extract is shown in Fig. 1. The positions of the peaks displayed in Fig. 1 and their attributions are as follows: 3378.89 cm^{-1}, O–H and N–H stretching vibrations; 2978.43 cm^{-1} and 2892.62 cm^{-1}, C–H stretching; 2112.15 cm^{-1}, N=C=S stretching; 1646.31 cm^{-1}, C=O

stretching; 1388.88 cm^{-1}, CH_3 bending; 1086.49 cm^{-1}, C=S stretching; and 1045.63 cm^{-1}, S=O stretching. The absorption bands below 1000 cm^{-1} correspond to aliphatic and aromatic C–H groups.

In summary, the SL extract contained polar groups based on N, O and S, such as O–H, N–H, C=O, C–O, C=S and S=O groups. Therefore, it was possible to prove simply that the SL extract had corrosion inhibition properties and could be used to inhibit the corrosion of metallic materials.

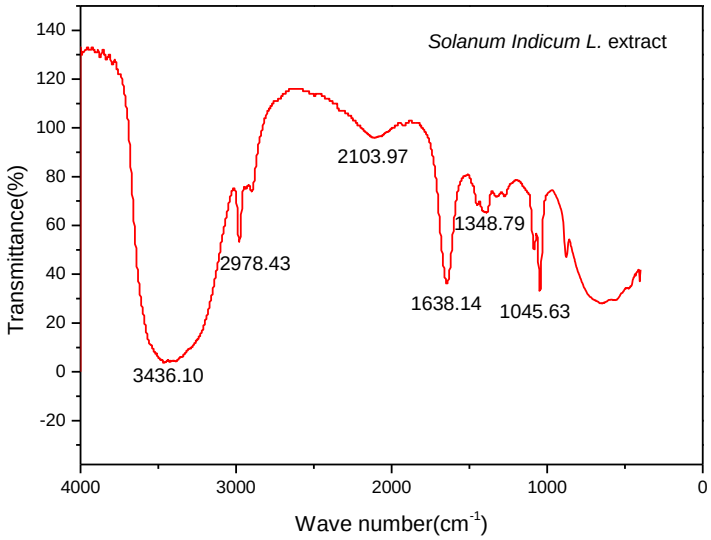

Figure 1. FTIR spectra of SL extract

3.3 Effects of temperature and concentration

Figures 2 and 3 show the experimental data for the weight loss of A3 steel in the 1 M HCl solution at different temperatures (30–60 °C) and different concentrations of the SL extract (0.2–1 g/L). The corrosion inhibition efficiency and corrosion rate were calculated by equations (1) and (2), respectively.

The trends in the corrosion rate with the temperature and concentration of the corrosion inhibitor are shown in Fig. 2. The corrosion rate of the A3 steel decreased with an increase in the SL extract concentration at the same temperature, and the minimum corrosion rate of 0.6 g m^{-2} h^{-1} was achieved when the optimal extract concentration of 1 g/L was employed at 303 K. This was because with the increase in the SL extract concentration more active molecules covered the surface of the A3 steel to form a denser film, and hence the corrosion rate was lower. When the concentration of the SL extract was the same, the corrosion rate of the A3 steel increased with an increase in temperature, which indicates that the temperature affected the inhibition efficiency of the corrosion inhibitor. This may have been caused by two factors. Firstly, because the movement of molecules is accelerated at a high temperature, the desorption rate of corrosion inhibitor molecules on the steel surface was greater than the adsorption rate. As a result, some corrosion inhibitor molecules were desorbed from the surface of the A3 steel, and part of the surface of the A3 steel was exposed to corrosion in a corrosive environment. Secondly, because high temperatures destroy the active ingredients in the SL extract, its corrosion-inhibiting effect was impaired.

The variable-temperature performance of the SL extract at different concentrations of 0.2–1 g/L in terms of inhibiting the corrosion of the A3 steel in the 1 mol/L HCl solution is shown in Fig. 3. It is

apparent that the corrosion inhibition efficiency increased as the concentration of the SL extract increased. This can be explained by the fact that as the concentration of the SL extract increased the adsorption of active molecules on the surface of the A3 steel was enhanced. Moreover, this indicates that the adsorption film that formed on the surface of the A3 steel at a high temperature was poorly protected. This was because the high temperature destroyed the active ingredients in the SL extract, and thus its corrosion-inhibiting effect decreased. In general, the SL extract was a highly effective corrosion inhibitor. In particular, when the temperature was 50 °C and its concentration was 1 g/L its inhibition efficiency reached 93.31%. Araújo Pereira *et al*.[11] studied the inhibitory action of an aqueous garlic peel extract on the corrosion of carbon steel in a 1 mol/L HCl solution. The results of weight loss measurements for the corrosion of carbon steel over 24 h at 25 °C show that η increased with an increase in the concentration of the garlic peel extract and varied from 32% to 96% in the concentration range of 10–1000 mg/L. Table 3 shows that SL extract has better corrosion inhibition effect at high temperature.

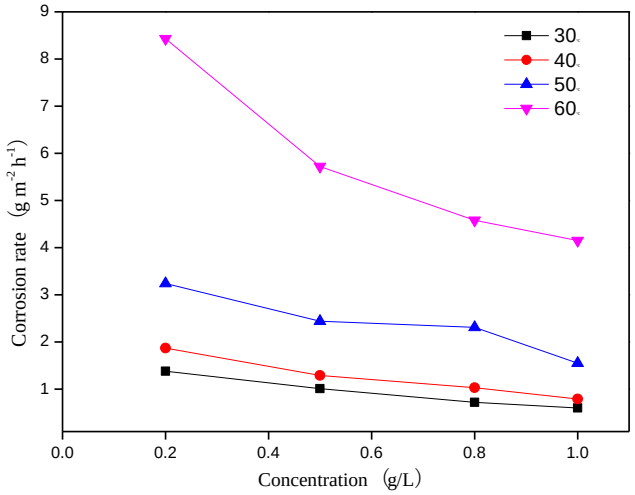

Figure 2. The corrosion rate of A3 steel varies with temperature and concentration of SL extract in 1 M HCl solution.

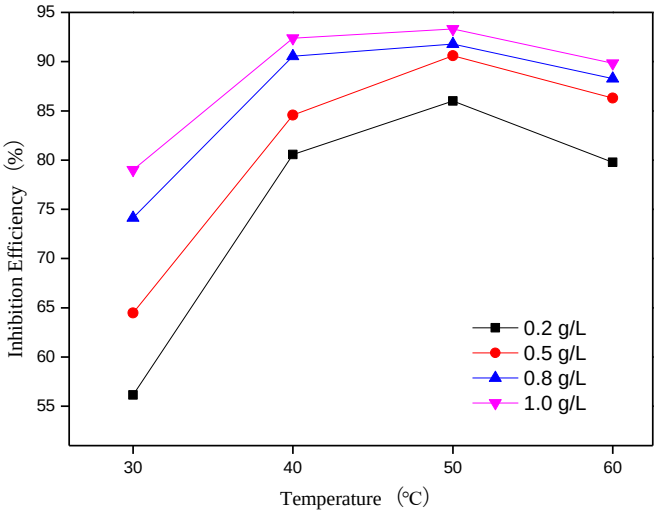

Figure 3. Trend of corrosion inhibition efficiency with temperature and concentration of SL extract in 1 M HCl solution

Table 3. Comparison of maximum corrosion inhibition efficiency of different plant corrosion inhibitors in 1M HCl solution

Inhibition	Temperature （°C）	Concentration （g/L）	Inhibition efficiency （%）
Solanum lasiocarpum L.	50	1.0	93.31
Aqueous garlic peel[11]	25	1.0	96.00
henna[30]	25	1.2	92.59
Pinus massoniana Needle[31]	25	0.8	95.00

3.4 Adsorption isotherms

The effective surface coverage (θ) of the inhibitor on the metal surface was calculated from the experimental data for weight loss; that is, θ is defined by:

$$\theta = \frac{\eta\%}{100} \quad (7)$$

The mechanism of corrosion inhibition may be explained on the basis of the adsorption behaviour[12]. The adsorption of SL on the surface of the A3 steel mainly corresponded to the Langmuir adsorption isotherm model. That is, the relationship between θ and the corrosion inhibitor concentration (C) could be expressed by the Langmuir adsorption isotherm.

$$\frac{C}{\theta} = \frac{1}{K_{ads}} + C \quad (8)$$

where C —— concentration of corrosion inhibitor , g/L

K_{ads} —— equilibrium constant of adsorption

θ —— surface coverage

Straight lines were obtained when C/θ was plotted against C (g/L) (Fig. 4). The linear correlation coefficient R^2 of the fitting curve was close to 1. The linear relationship indicates that the adsorption of corrosion inhibitor molecules in the SL extract on the surface of the A3 steel conformed to the Langmuir adsorption isotherm. Odewunmi *et al*.[13] studied the utilization of a watermelon rind extract (WMRE) as a green corrosion inhibitor for mild steel in two acidic media. WMRE was found to be physically adsorbed on the mild steel surface in both acidic media according to the Temkin adsorption isotherm model. Table 4 shows that the adsorption of plant inhibitors mainly obeyed Langmuir and Temkin adsorption isotherms model.

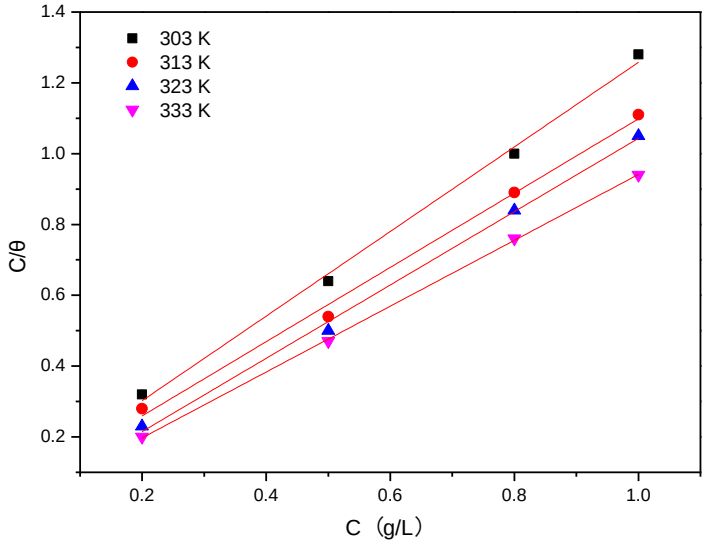

Figure 4. Langmuir adsorption plots of SL extract on the A3 steel in 1 M HCl solution.

Table 4. Comparison of adsorption isothermal models for different plant corrosion inhibitors

Inhibition	Adsorption isotherm model
Solanum lasiocarpum L.	Langmuir
Watermelon rind[13]	Temkin
Gingko biloba fruit [17]	Langmuir
Hydroclathrus clathratus marine alga[20]	Temkin
Kleinia grandiflora leaf [24]	Langmuir
Coconut coir [32]	Temkin

Table 5. Thermodynamic parameters for adsorption of SL extract onto the A3 steel surface in 1 M HCl solution at different temperatures

T K	K_{ads}	ΔG_{ads} KJ mol^{-1}	ΔH_{ads} KJ mol^{-1}	ΔS_{ads} J mol^{-1} K^{-1}	R^2
303	15.8	-17.1	-54.1	-122.3	0.995
313	20.3	-18.3		-114.5	0.994
323	126.7	-23.8		-94.0	0.996
333	88.6	-23.5		-91.9	0.999

The adsorption equilibrium constant K_{ads} was calculated from the intercept of the straight line in Fig. 4, and the results of the calculation are shown in Table 5. The relationship between the adsorption free energy (ΔG_{ads}) and K_{ads} is shown in equation (9), whereby the value of ΔG_{ads} can be calculated.

$$\Delta G_{ads} = -RT\ln(55.5 \times K_{ads}) \quad (9)$$

where R —— gas constant

T —— temperature

55.5 —— molar concentration of water

It was found that the value of K_{ads} first increased and then decreased with an increase in temperature and reached a maximum at a temperature of 323 K. This indicates that the interaction between the adsorbed molecules and the metal surface first strengthened and then weakened as the temperature increased. The corrosion inhibition efficiency first increased and then decreased with an increase in temperature, which was consistent with the results for the weight loss.

(1) The negative values of ΔG_{ads} clearly indicated that the adsorption of the SL extract on the A3 steel surface was spontaneous and the adsorbed layer on the A3 steel surface was stable[14,15]. Moreover, the large negative values of ΔG_{ads} suggest that the active molecules in the SL extract had a strong tendency to be adsorbed on the A3 steel surface in the acidic solution[16], which was consistent with the results of the weight loss experiment. In general, values of ΔG_{ads} of ≤ -20 kJ mol^{-1} signify physisorption, and values that are more negative than -40 kJ mol^{-1} signify chemisorption[17–19]. In the present study, the calculated value of ΔG_{ads} for the SL extract was in the range from -23.5 kJ mol^{-1} to -17.1 kJ mol^{-1} (Table 5), which probably implies that both physisorption and chemisorption (comprehensive adsorption) took place, but the adsorption of the SL extract on the surface of the A3 steel mainly involved physisorption. In addition, this indicates that the adsorption behaviour was consistent with the electrostatic interaction between a charged molecule and a charged metal. Kamal *et al*.[20] studied the marine alga *Hydroclathrus clathratus* as a green inhibitor of the acid corrosion of mild steel. The ΔG_{ads} values that were determined were less than -20 kJ mol^{-1}, which indicated the physisorption of inhibitor molecules onto the mild steel surface. As shown in Table 6, the adsorption process of plant corrosion inhibitors involved both physisorption and chemisorption, but mainly physisorption.

Table 6. Comparison of adsorption process of different plant corrosion inhibitors

Inhibition	**$\lvert\Delta G_{ads}\rvert$(KJ mol^{-1})**	**Adsorption process**
Solanum lasiocarpum L.	17.1–23.5	Physisorption and Chemisorption
Gingko biloba fruit[17]	31.3	Physisorption and Chemisorption
Hydroclathrus clathratus marine alga[20]	18.96 –19.03	Physisorption
Kleinia grandiflora leaf [24]	18.28–18.40	Physisorption

The adsorption enthalpy (ΔH_{ads}) and adsorption entropy (ΔS_{ads}) were used to explain the adsorption of inhibitor molecules at the metal/solution interface. The value of ΔH_{ads} was calculated using the van't Hoff equation.

$$\ln K_{ads} = -\frac{\Delta H_{ads}}{RT} + \frac{\Delta S_{ads}}{R} + \ln 55.5 \quad (10)$$

The linear relationship between ln K_{ads} and 1000/T is shown in Fig. 5. From equation (10), it is known that the slope of this line is equal to $-\Delta H_{ads}/R$, where R is the gas constant, from which ΔH_{ads} can be calculated. The value of ΔS_{ads} can be calculated by the basic equation of thermodynamics.

$$\Delta S_{ads} = \frac{\Delta H_{ads} - \Delta G_{ads}}{T} \quad (11)$$

The values of all the thermodynamic parameters, such as ΔH_{ads} and ΔS_{ads}, are listed in Table 5. The value of ΔH_{ads} was negative, which indicates that the adsorption of corrosion inhibitor molecules in the SL extract on the metal surface was exothermic. That is, corrosion inhibitor molecules in the SL extract were gradually desorbed from the surface of the A3 steel at high temperatures, which resulted in a decrease in corrosion inhibition efficiency[12]. The negative value of ΔS_{ads} indicates that the adsorption process was exothermic and involved an increase in entropy. An increase in the amount of adsorbed material led to an increase in the degree of chaos in the solution. The active material replaced water molecules and was then adsorbed on the surface of the A3 steel to form an adsorption layer, which inhibited the corrosion of the A3 steel.

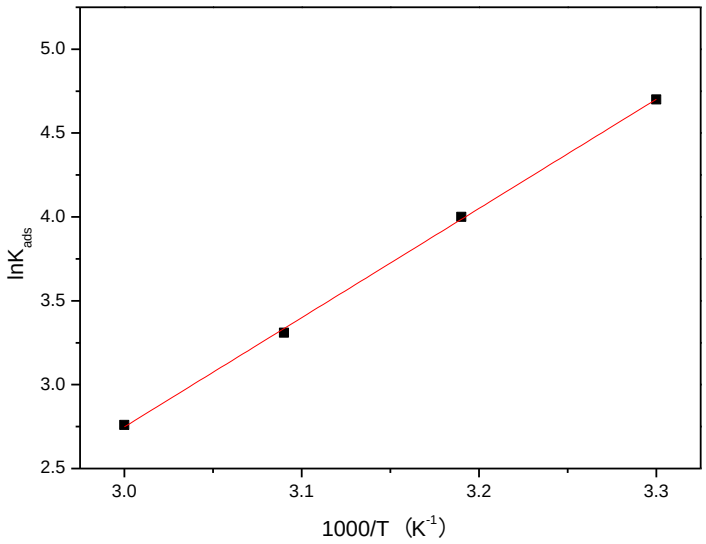

Figure 5. Plot of lnK_{ads} versus 1/T for the adsorption of SL extract at A3 steel/HCl interface.

3.5 Activation parameters of the inhibition process

For different temperatures (303–333 K) and concentrations of the SL extract (0.2–1 g/L), the apparent activation energy (E_a), enthalpy of activation (ΔH^*) and entropy of activation (ΔS^*) were calculated by the Arrhenius and transition state equations:

$$\log V_{corr} = \log A - \frac{E_a}{RT} \quad (12)$$

$$\log\left(\frac{V_{corr}}{T}\right) = \log\left(\frac{R}{hN_A}\right) + \left(\frac{\Delta S^*}{R}\right) - \left(\frac{\Delta H^*}{RT}\right) \quad (13)$$

where T is the temperature, h is Planck's constant, N_A is Avogadro's number and R is the gas constant (8.314 J mol^{-1} K^{-1}).

The value of E_a was calculated from the slope of plots of lg V_{corr} vs 1000/T, where V_{corr} represents the corrosion rate, as shown in Fig. 6; the slope of such a plot is $-E_a/R$. Plots of lg (V_{corr}/T) vs 1000/T give a straight line with a slope of $-\Delta H^*/R$ and an intercept of lg (R/hN_A) + $\Delta S^*/R$, as shown in Fig. 7. The values of ΔH^* and ΔS^* can be calculated from the slope and intercept of the straight line, respectively. The values of all the activation parameters, such as E_a, ΔH^* and ΔS^*, are listed in Table 7.

The value of E_a was higher than that of the blank solution after the addition of the corrosion inhibitor, which indicated that the adsorption of the corrosion inhibitor mainly comprised physisorption[21,22]. According to the value of E_a in Table 7, the adsorption of the SL extract mainly involved physical adsorption. The value of E_a increased with an increase in the concentration, which indicates that more active molecules in the SL extract were adsorbed on the metal surface. In addition, this indicates that the energy required for the reaction increased, the difficulty of the corrosion reaction increased and the corrosion inhibition efficiency increased. This can be explained by the fact that the central atoms in the inhibitor molecules in the SL extract had a common pair of electrons, which coordinated with H^+ ions to form cations. These cations were adsorbed on the cathode region of the metal surface under the influence of electrostatic forces, which resulted in positive charges at the interface and prevented H^+ ions from approaching the metal surface in the solution and thus prevented the corrosion reaction.

The value of ΔH^* was positive, which indicates that the dissolution of the A3 steel was an endothermic process, which requires more energy to reach an effective or equilibrium state. The value of ΔH^* increased as the concentration of the SL extract increased. This indicates that the energy required for the corrosion reaction of the A3 steel increased when the concentration of the SL extract increased, the barrier to the corrosion reaction increased and the corrosion rate of the metal decreased. This was due to the adsorption of corrosion inhibitor molecules in the SL extract on the metal surface. It is clear that the value of ΔS^* increased in the presence of the SL extract. For the free acidic solution, this can be explained as follows: the transition state in the rate-determining recombination step represented a more orderly arrangement with respect to the initial state, and hence a high value of ΔS^* was attained[12]. Because the surface was covered with inhibitor molecules, the discharge of H^+ ions from the metal surface was retarded, which caused the system to pass from a random arrangement, and hence the value of ΔS^* increased. This indicates an increase in disorder due to the adsorption of inhibitor molecules as a result of the desorption of more water molecules.

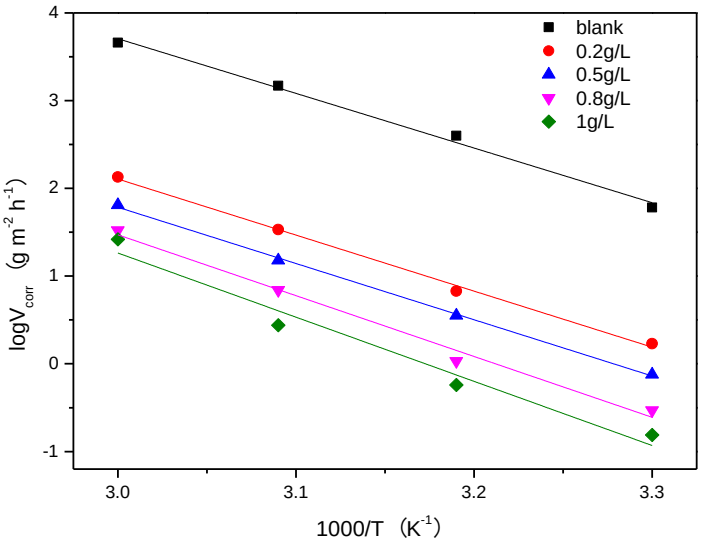

Figure 6. Arrhenius plots for $\log V_{corr}$ vs 1000/T for A3 steel in 1 M HCl solution at different concentration of SL extract

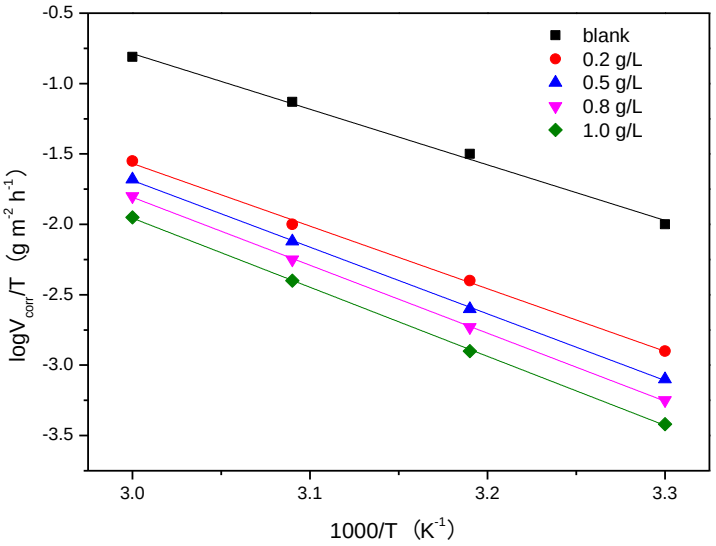

Figure 7. The relationship between $\log V_{corr}/T$ vs 1000/T for A3 steel at different concentrations of SL extract

Table 7. Activation parameters of the A3 steel in 1M HCl solution in the absence and presence of different concentrations of SL extract

Concentration g/L	**E_a KJ mol^{-1}**	**ΔH^* KJ mol^{-1}**	**ΔS^* J mol^{-1}K^{-1}**	**R^2**
0	51.8	32.8	-105.6	0.994
0.2	53.1	36.9	-99.7	0.997
0.5	53.3	39.4	-93.5	0.999
0.8	57.7	40.2	-92.2	0.999
1	60.8	40.8	-91.4	0.999

3.6 Electrochemical impedance spectroscopy

Nyquist plots for the A3 steel in the 1 M HCl solution in the absence and presence of various concentrations of the SL extract are presented in Fig. 8. The impedance response was represented by semicircles of capacitive type. This was because the adsorption of the corrosion inhibitor on the electrode surface resulted in an increase in R_{ct}, so that the dissolution of the anode metal became difficult and the corrosion resistance of the electrode increased. After the addition of the SL extract, the shape of the impedance spectrum curve was similar, which indicated that the corrosion mechanism of the A3 steel was not changed by the addition of the extract.

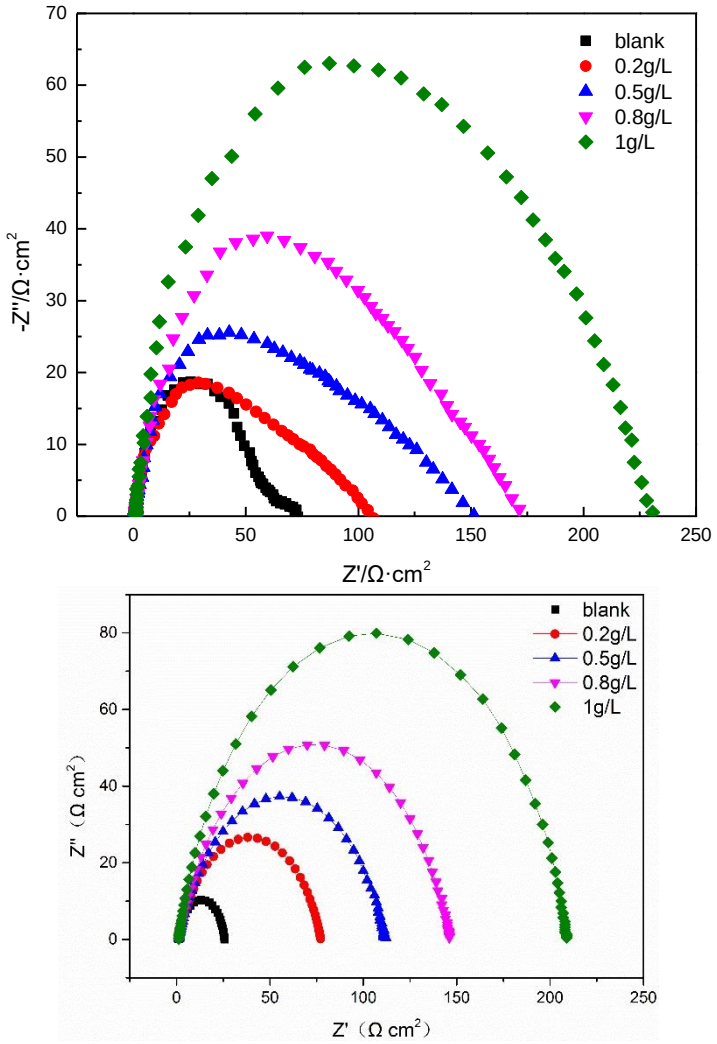

Figure 8. Nyquist plots for the A3 steel in 1M HCl Solution in the absence and presence of different concentrations of SL extract at 303K

The results of the electrochemical impedance spectroscopy experiments are shown in Table 8. R_s is the solution resistance, R_{ct} is the charge transfer resistance and C_{dl} is the double-layer capacitance. The increase in R_{ct} was due to the gradual replacement of water molecules as a result of the adsorption of chemical constituents of the SL extract at the metal/solution interface[23,24]. This caused corrosion inhibitor molecules to form a protective film on the surface of the A3 steel, which then limited the extent

of the dissolution reaction. It is shown that R_{ct} increased gradually, which implies that the corrosion inhibition efficiency also increased gradually. The value of η was calculated using equation (4). When the temperature was 30 °C and the SL extract concentration was 1 g/L, the corrosion inhibition efficiency reached 88.2%.

Table 8. Electrochemical impedance parameters for the A3 steel in 1M HCl Solution in the absence and presence of different concentrations of SL extract at 303K

Concentration(g/L)	R_s(Ω▪cm^2)	R_{ct} (Ω▪cm^2)	C_{dl}(F▪cm^{-2})	η(%)
Blank	1.2	24.5	1.4×10^{-3}	-
0.2	1.3	76.0	3.2×10^{-4}	67.8
0.5	1.2	110.6	2.4×10^{-4}	77.9
0.8	1.1	145.3	2.3×10^{-4}	83.2
1	1.0	207.8	9.1×10^{-5}	88.2

3.7 Potentiodynamic polarization measurements

The polarization behaviour of the A3 steel in the 1 M HCl solution in the absence and presence of the SL extract at 303 K is shown in Fig. 9. As can be seen from Fig. 9, both the anodic and the cathodic portions of the curve are offset in the negative direction, which indicates that the bipolar reactions were effectively suppressed. That is, the SL extract had an inhibitory effect on the anodic dissolution reaction and the cathodic hydrogen evolution reaction of the A3 steel. The values of all the polarization parameters, such as I_{corr}, E_{corr}, β_c and β_a, are listed in Table 9. The value of η was calculated using equation (3), as shown in Table 9. From Table 9, it can be seen that as the SL extract concentration increased, the value of I_{corr} gradually decreased and the corrosion inhibition efficiency increased and reached a maximum of 82.5% at a concentration of 1 g/L.

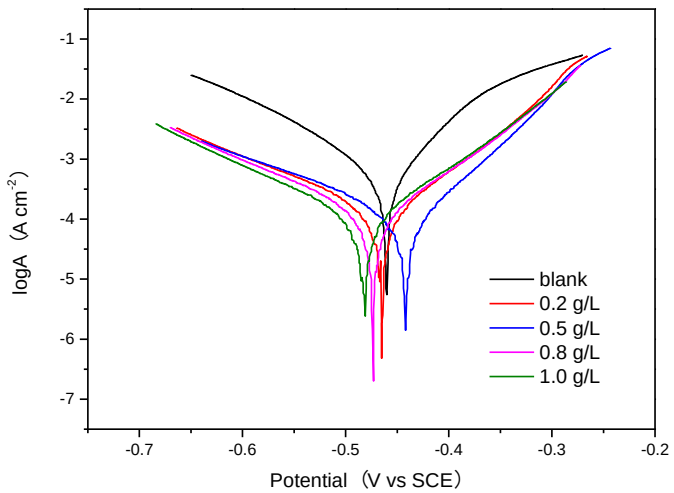

Figure 9. Potentiodynamic polarization curves for the A3 steel in 1M HCl solution in the absence and presence of different concentrations of SL extract at 303K.

Table 9. Polarization parameters and corresponding inhibition efficiency for the corrosion of A3 steel in 1M HCl solution containing different concentrations of SL extract at 303K.

Concentration g/L	$-E_{corr}$ mV	I_{corr} μA cm^{-2}	β_a mV/decade	$-\beta_c$ mV/decade	η %
blank	460.4	615.0	79.4	110.2	-
0.2	465.1	120.2	85.2	135.6	80.1
0.5	447.8	113.2	97.6	136.3	81.6
0.8	473.5	109.0	94.2	130.8	82.3
1	476.4	107.9	91.9	136.2	82.5

The decrease in I_{corr} on the addition of the inhibitor suggested the formation of a protective layer over the metal surface[25]. A change in the E_{corr} value was also observed in the presence of the SL extract. If the change in the E_{corr} value is less than 85 mV, the inhibitor is considered to be a mixed-type inhibitor[26,27]. In the present study, the maximum change in the E_{corr} value was 16 mV, which indicates that this corrosion inhibitor exhibited mixed-type inhibition. No significant change in the value of E_{corr} occurred, which indicates that the geometrical blocking effect in the adsorption process was stronger than the energy effect; that is, the adsorption process mainly involved a geometrical blocking mechanism[22]. Behpour *et al*.[28] studied a green approach for inhibiting the corrosion of mild steel in two acidic solutions using an extract of *Punica granatum* peel and its main constituents. Potentiodynamic polarization curves indicated that *Punica granatum* extract and ellagic acid behaved as mixed-type inhibitors.

In order to further determine the type of corrosion inhibition exhibited by the SL extract, the anodic interaction coefficient f_a and cathodic interaction coefficient f_c were calculated using equations (14) and (15), respectively, according to the polarization curve parameters, as shown in Table 10.

$$f_a = \frac{I_{corr(inh)}}{I_{corr}} \exp\left(\frac{E_{corr} - E_{corr(inh)}}{b_a}\right) \quad (14)$$

$$f_c = \frac{I_{corr(inh)}}{I_{corr}} \exp\left(\frac{E_{corr(inh)} - E_{corr}}{b_c}\right) \quad (15)$$

The values of f_a and f_c in Table 10 are less than 1, which indicates that the adsorbed inhibitor molecules affected both the anodic reaction and the cathodic reaction. Moreover, for the same inhibitor, the lower is the value of f_a or f_c, the stronger is the inhibiting effect of the inhibitor. The ratio of f_a to f_c was greater than 1[29], which indicates that at the same concentration the SL extract inhibitor inhibited the cathodic reaction to a greater extent than the anodic reaction, and hence this inhibitor acted as a hybrid inhibitor with dominant cathodic inhibition. With an increase in the SL extract concentration, both f_a and f_c decreased gradually, and the corrosion-inhibiting effect of the corrosion inhibitor increased. This indicates that the higher is the SL extract concentration, the higher is the corrosion inhibition efficiency.

Table 10. The interaction coefficient of SL extract on A3 steel

concentration g/L	f_a	f_c	f_a/f_c
0.2	0.2065	0.2023	1.0208
0.5	0.2048	0.1974	1.0374
0.8	0.2037	0.1959	1.0398
1	0.2022	0.1912	1.0575

3.8 SEM analysis

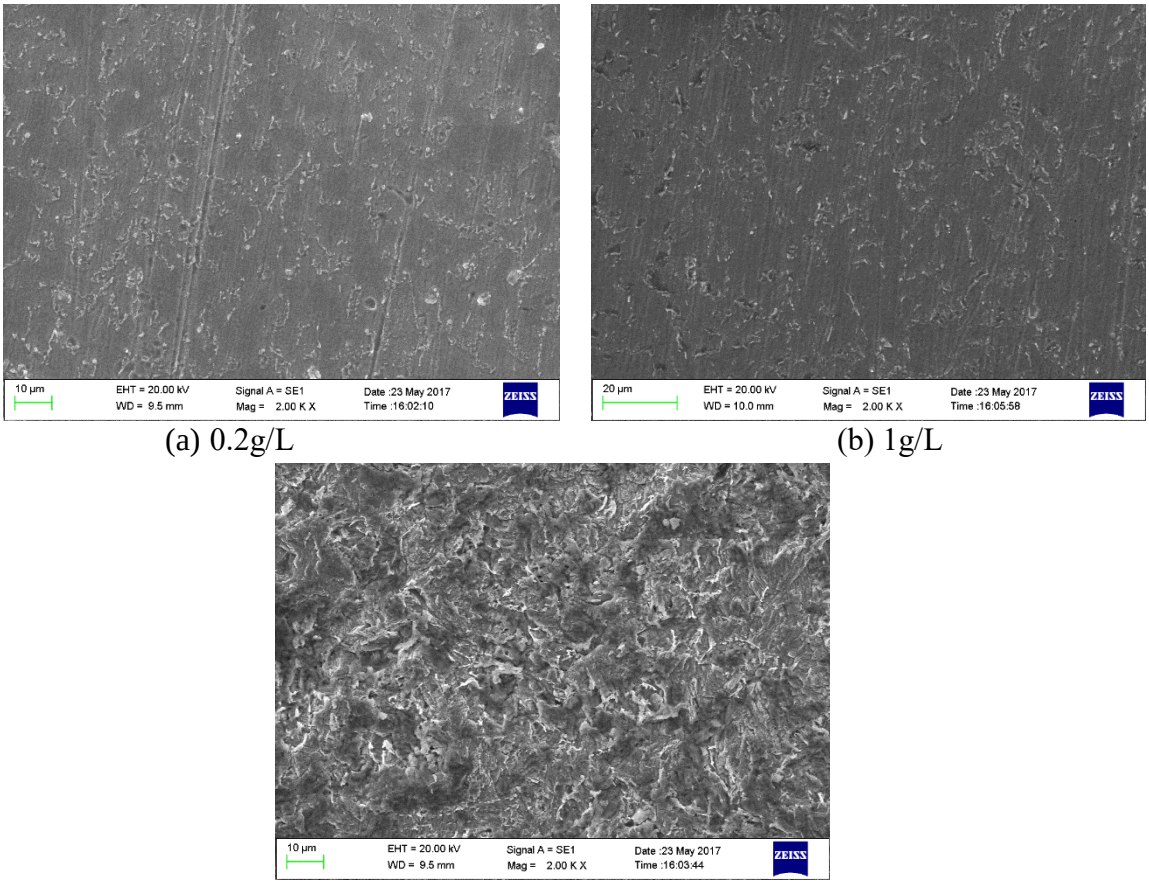

(a) 0.2g/L (b) 1g/L

(c) blank

Figure 10. Surface morphology of A3 steel after adding different concentrations of SL extract at 50°C and 1mol/L HCl solution

SEM images of the polished A3 steel surface and the A3 steel immersed in 1 M HCl in the absence and presence of the SL extract are shown in Fig. 10(a–c). From Fig. 10(a), it can be seen that in the absence of the SL extract the surface of the A3 steel was uneven and there were a large number of corrosion pits. After the addition of the SL extract, the number of corrosion pits on the surface of the A3 steel was significantly reduced and the surface became smooth, which indicates that the SL extract effectively inhibited the corrosion of the A3 steel in the 1 mol/L HCl solution. This observation indicates

that the corrosion rate decreased remarkably in the presence of the inhibitor. This might have been due to the adsorption of inhibitor molecules on the metal surface in the form of a protective layer. When the concentration was 1 g/L, the A3 steel surface had fewer corrosion pits and was smoother, which indicates that with an increase in the SL extract concentration the corrosion-inhibiting effect was stronger.

4. CONCLUSIONS

(2) The optimum conditions for the preparation of the SL extract were as follows: a soaking temperature of 343 K, a soaking time of 16 h and an ultrasound time of 60 min.

(3) The SL extract contained polar groups based on N, O and S. Substances containing these polar groups could be used to determine the inhibition performance of the SL extract.

(4) When the temperature was 303 K and the corrosion inhibitor concentration was 1 g/L, the corrosion rate reached its minimum value of 0.6 g m^{-2} h^{-1}. When the temperature was 323 K and the corrosion inhibitor concentration was 1 g/L, the corrosion inhibition efficiency reached 93.31%.

(5) The adsorption of the SL extract on the surface of the A3 steel obeyed the Langmuir adsorption isotherm model and comprised the adsorption of a single molecular layer. The adsorption process involved both physisorption and chemisorption, but mainly physisorption.

(6) The SL extract is a hybrid corrosion inhibitor that predominantly suppresses the cathodic reaction.

ACKNOWLEDGEMENTS
This work was supported by the National Natural Science Foundation of China (No. 51774242).

References

1. K.K. Hu, Q.D. Li, Z.C. Meng and B. Wang, *Corros Sci Prot Technol.*, 28(2016)577.
2. EE Oguzie, *Corros. Sci.*, 50 (2008)2993.
3. X.D. Zhang, G. Yu, F. Xu, *Contemp Chem Ind.*, 45(2016)279.
4. E Rodriguez-Clemente, JG Gonzalez-Rodriguez, G Valladarez and GF Dominguez-Patiño, *Int. J. Electrochem. Sci.*, 6 (2011) 6360.
5. X. Wang, F.Y. Wang, Y.X. Chen, X.X. Ji, S.C. Shi, *Corros Sci Prot Technol.*, 29(2017)85.
6. J. Zheng, Y.N. Wang, B.L. Zhang, T.Yang, X.M. Jiao and Y. He, *Corros Sci Prot Technol.*, 23(2011) 103.
7. J.X. Wen, Y.X. Liu, J.Y. Yao, Y.F. Zhou, *Mater Prot.*, 50(2017)20.
8. X.H. Li, S.R. Deng, X.G. Xie and G.B. Du, *Acta Phys-Chim Sin.*, 30(2014)1883.
9. Syu W., Don M., Lee G., Sun C., J. Nat. Prod., 64(2001)1232.
10. Mona EL-A ASR, Hiroyuki MIYASHITA, Tsuyoshi IKEDA, Jong-Hyun LEE, Hitoshi Y OSHIMITSU , Toshihiro NOHARA and Kotaro MURAKAMI, *Chem. Pharm. Bull.*, 57(2009) 747.
11. Pereira. SSDA, Pegas. MM, Fernandez. TL, Magalhaes. M and Schontag. TG, *Corros. Sci.*, 65(2012)360.
12. P. Muthukrishnan, P. Prakash, B. Jeyaprabha and K. Shankar, *Arabian J. Chem.*, (2015)1878.
13. N.A. Odewunmi, S.A. Umoren and Z.M. Gasem, *J. Ind. Eng. Chem.*, 21(2015)239.
14. M.A.Quraishi, D.Jamal, Mater. *Chem. Phys.*, 78(2003)608.

15. OK Abiola, NC Oforka, EE Ebenso and NM Nwinuka, *Anti-Corros. Methods Mater.*, 54 (2007) 219.
16. Chandra Bhan Verma, M.A. Quraishi, Ambrish Singh, *J Taiwan Inst Chem E.*, 49(2015)229.
17. Ambrish Singh, Yuanhua Lin, Eno. E. Ebenso, Wanying Liu, Jie Pan and Bo Huang, *J. Ind. Eng. Chem.*, 24 (2015) 219.
18. M.M. Solomon, S.A. Umoren, I.I. Udosoro and A.P. Udoh, *Corros. Sci.*, 52 (2010) 1317.
19. S.A. Umoren, I.B. Obot, E.E. Ebenso and N.O. Obi-Egbedi, *Desalination*, 247(2009) 561.
20. C. Kamal, M. G. Sethuraman, *Res. Chem. Intermed.*, 39(2013)3813.
21. F Bentiss, M Lebrini, M Lagrenee, *Corros.Sci.*, 47(2005)2915.
22. Li xianghong, Fu hui, Deng shuduan, *J Chin Soc Corros Prot.*, 31(2011)149.
23. K.F. Khaled, *Electrochim. Acta*, 48(2003)2493.
24. Muthukrishnan Pitchaipillai , Karthik Raj , Jeyaprabha Balasubramanian and Prakash Periakaruppan, *Int. J. Miner., Metall. Mater.*, 21(2014)1083.
25. C. Kamal, M.G. Sethuraman, *Res. Chem. Intermed.*, 39(2013)3813.
26. E.S. Ferreira, C. Giancomelli, F.C. Giacomelli, and A. Spinelli, *Mater. Chem. Phys.*, 83(2004)129.
27. M. Xia, P.L. Guan, K. Gong,X.Y. Sun, F. Ren and D.F. Shen, *Corros Sci Prot Technol.*, 6(2013)495.
28. M. Behpour, S.M. Ghoreishi, M. Khayatkashani and N. Soltani, *Mater. Chem. Phys.*,131(2011)621.
29. C.N. Cao, Electrochemical corrosion principle, *Chemical Industry Press*, (2004)Beijing, China.
30. A. Ostovari, S.M. Hoseinieh, M. Peikari, S.R. Shadizadeh and S.J. Hashemi, *Corros.Sci.*, 51(2009)1935.
31. X. Wang, S.F. Ren, D.X. Zhang, H. Jiang and Y. Gu, *Int. J. Electrochem. Sci.*, 13 (2018) 9888.
32. S.A. Umoren, I.B. Obot, A.U. Israel, P.O. Asuquo, M.M. Solomon, U.M. Eduok and A.P. Udoh, *J. Ind. Eng. Chem.*, 20(2014)3612.